JOURNAL OF GEOPHYSICAL RESEARCH: OCEANS, VOL. 118, 4585–4599, doi:10.1002/jgrc.20333, 2013

# Wind-driven exchanges between two basins: Some topographic and latitudinal effects

Jiayan Yang,[1] Xiaopei Lin,[1,2] and Dexing Wu[2]

Received 29 April 2013; revised 29 July 2013; accepted 31 July 2013; published 18 September 2013.

[1] This study examines some topographic effects on the *island rule*. We use an idealized and barotropic model to investigate the throughflow between a semienclosed marginal sea and a larger oceanic basin that are connected to each other by two channels. Two sets of experiments are conducted in parallel, one with a flat bottom and the other with a ridge between two basins. The model results show that the ridge affects the island rule considerably in several ways. First, the ridge blocks geostrophic contours and restricts a free exchange between two basins. The bottom pressure torque (or the form drag) is a dominant term in the balance of the depth-integrated vorticity budget and always results in a significant reduction of the throughflow transport. Second, horizontal friction promotes cross-isobathic flows and enhances the throughflow transport over the ridge. This is the opposite of what friction does in the original island rule in which a friction tends to reduce the throughflow transport. Third, the forcing region in the open ocean for the marginal-sea throughflow is shifted meridionally. Last, the topographic effect becomes small near the equator due to its dependence on $f$. This may explain why the PV barrier effect is smaller in the South China Sea than in the Japan/East Sea. The limitation of the barotropic model and some baroclinic effects will be discussed.

**Citation:** Yang, J., X. Lin, and D. Wu (2013), Wind-driven exchanges between two basins: Some topographic and latitudinal effects, *J. Geophys. Res. Oceans*, *118*, 4585–4599, doi:10.1002/jgrc.20333.

## 1. Introduction

[2] Flows between two oceanic basins, such as the Indonesian througflow (ITF), are important components of the global ocean circulation. But making in situ observations can be difficult in some passages due to restrictions by their bordering countries. It is, therefore, desirable to develop a method for estimating throughflow transports from more available observations, like wind stress over the open ocean. In a seminal study, *Godfrey* [1989] derived a solution, which has been commonly called the *island rule (IR)*, and applied it with some success to the ITF. In a steady state, the ITF is essentially a flow around a big island—Australia. The presence of an island provides some mathematical and dynamical conveniences in deriving a balance of vorticity flux that ties the ITF transport to the wind stress over the Pacific Ocean. In the original IR, Godfrey used a steady, linear, and wind-driven circulation model. Topographic effects were not considered explicitly.

[3] The IR has been tested in some marginal seas where topographic variations are large, such as in the Japan/East Sea (JES) and the South China Sea (SCS) (Figure 1a). It comes with no surprise that the IR fell apart when applied to the Tsushima Warm Current (TSWC) since two main throughflow straits, the Tsushima and Tsugaru Straits, are shallower than 200 m [*Seung*, 2003]. The observed TSWC transport, about 2 and 3 Sv [*Ohshima*, 1994; *Takikawa et al*., 2005], is one order of magnitude smaller than what would be estimated by using the IR. The disparity between the observed and IR-inferred transports in the SCS, however, is much smaller [*Qu et al*., 2005; *Wang et al*., 2006a, 2006b] even though the main exit straits for the SCS throughflow (SCSTF) are very shallow. The SCSTF enters the SCS through the Luzon Strait but exits mainly through the Karimata Strait (<50 m in depth, marked by 6 in Figure 1a) and the Mindoro Strait (<200 m, marked by 5 in Figure 1a). Regardless the IR applicability there, one would expect that the same topographic barrier effects that restrict the applicability of the IR in the TSWC would remain effective in the SCS case. Why is the topographic restriction smaller in the SCS?

[4] Few studies have examined the role of topography in the context of the IR and some fundamental issues remain to be explored. In this study, we will focus on barotropic flows with a goal of developing some dynamical insights that can be applied to three-dimensional models. Some potential effects of baroclinic processes will be discussed in section 6. While this study is motivated partly by some aspects of the JES and SCS throughflows, we are interested

[1]Department of Physical Oceanography, Woods Hole Oceanographic Institution, Woods Hole, Massachusetts, USA.
[2]Physical Oceanography Laboratory, Ocean University of China, Qingdao, China.

Corresponding author: J. Yang, Department of Physical Oceanography, Woods Hole Oceanographic Institution, Woods Hole, MA 02543, USA. (jyang@whoi.edu)


2169-9275/13/10.1002/jgrc.20333

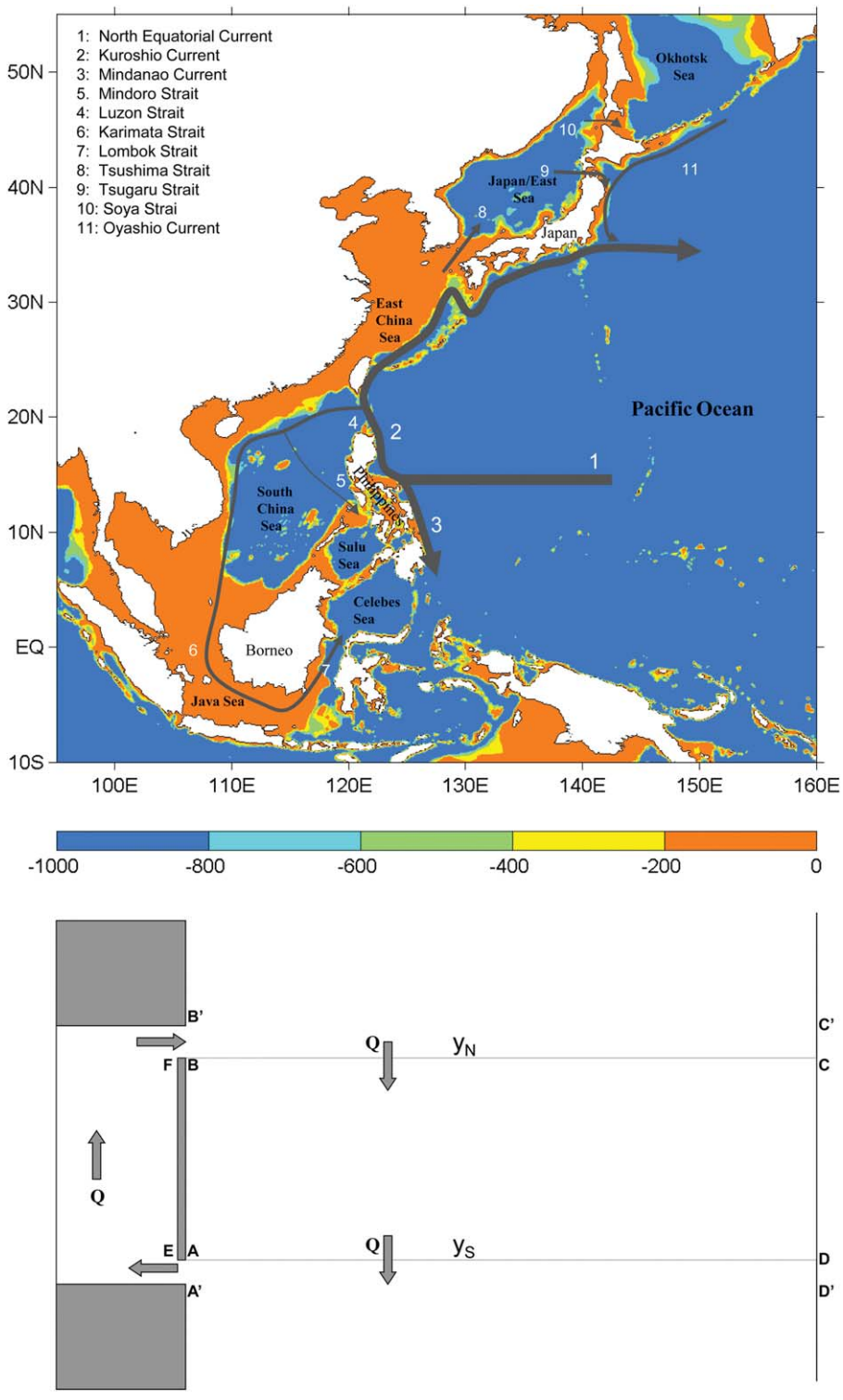


**Figure 1.** (top) The bathymetry of the Northwestern Pacific Ocean between the JES and SCS with schematics of major currents in the region. The SCS throughflow pathways are from *Qu et al*. [2005]. (bottom) Schematic of the island rule integration. In the classic island rule [*Godfrey*, 1989], the transport around the island depends solely on the wind stress along the close line $l = CBFEADC$ and the planetary vorticity difference between the two extremities of the island, $y_N$ and $y_S$. It will be shown in this study that the topography, if it blocks the PV contours between two deep basins, can dramatically reduce the transport of the island and is the leading cause for the difference between the observed Tsushima Warm Current (TSWC) transport and the island rule estimated transport. Our idealized model domain is closed and, therefore, ignores the net transport through Bering Strait (∼0.8 Sv) [*Woodgate and Aagaard*, 2005].

in a more general marginal-sea throughflow and will use idealized bathymetry and forcing. The real applicability of the IR in both JES and SCS depends on many other factors that are beyond the scope of this study.

[5] This paper is organized as follows. In section 2, we will review the IR and discuss some topographic effects. In section 3, a barotropic model and its results will be presented to examine some effects of topography and friction. In section 4, we will discuss how the area of the open-ocean forcing is shifted when a ridge is placed between two basins. We will discuss, in section 5, the latitudinal dependence of the topographic effects and explain why topographic effects weaken in low-latitude marginal seas. The limitation of our results from a barotropic model and potential effects from stratification will be discussed in section 6. A summary will be given in section 7.

## 2. The Island Rule

[6] Here we will review the derivation of Godfrey's IR and extend it to include some topographic effects. Consider a stratified ocean in an idealized domain like the one that is shown in Figure 1b. A meridionally elongated island lies between a marginal sea and an open oceanic basin. The depth-integrated vorticity equation is:

$$\frac{\partial Z}{\partial t}+\nabla\cdot\left[\vec{U}(f+\zeta)\right]=-\frac{1}{\rho_0}curl_z(h\nabla p_b)+\frac{1}{\rho_0}curl_z\left(\overrightarrow{\tau_w}-\overrightarrow{\tau_f}\right) \tag{1}$$

where $\vec{U}=\int_{-h}^{0}\vec{u}dz$ is the vertically integrated velocity, $Z=curl_z\vec{U}$ is the vertical curl of the vertically integrated velocity, $\zeta=v_x-u_y$ is the relative vorticity, $\vec{k}$ is the unit vector in the vertical direction, $h$ is the depth of the water column, $p_b$ is the pressure on the bottom surface, and $\overrightarrow{\tau_w}$ and $\overrightarrow{\tau_f}$ are the wind stress and the friction, respectively. The first term on the right-hand side of equation (1) is the bottom pressure torque (or the form drag) that vanishes in a flat-bottom model. Both the topographic (through $h$) and baroclinic (through $p_b$) effects appear in this bottom pressure torque term. Baroclinic processes also affect the bottom friction because it is induced by a bottom velocity that consists of both barotropic and baroclinic components.

[7] Follow *Pedlosky et al*. [1997], we can integrate the vorticity equation (1) over the area bounded by *CBADC* in Figure 1b (the area to the east of the island's east coast) and use an integration of the depth-integrated momentum equations around the island *BAEFB*. The combined of these two integration yields:

$$\oint_l(f+\zeta)(\vec{U}\cdot\vec{n})ds=-\oint_l\frac{h}{\rho_0}\left(\nabla p_b\cdot\vec{l}\right)ds+\oint_l\left(\frac{\overrightarrow{\tau_w}-\overrightarrow{\tau_f}}{\rho_0}\cdot\vec{l}\right)ds \tag{2}$$

where $l=CBFEADC$ is the integration path in equation (2) and $\vec{n}$ is the unit vector perpendicular to the integration path $l$. If the Rossby number is small, the nonlinear term is negligible and equation (2) becomes:

$$\oint_l f(\vec{U}\cdot\vec{n})ds\approx-\oint_l\frac{h}{\rho_0}\left(\nabla p_b\cdot\vec{l}\right)ds+\oint_l\left(\frac{\overrightarrow{\tau_w}-\overrightarrow{\tau_f}}{\rho_0}\cdot\vec{l}\right)ds \tag{3}$$

[8] The left-hand side term can be rewritten as:

$$\oint_l f(\vec{U}\cdot\vec{n})ds=\left(\int_{AD}+\int_{DC}+\int_{CB}+\int_{BFEA}\right)\left[f(\vec{U}\cdot\vec{n})\right]ds=(f_N-f_S)Q$$

[9] Note that the integration along the solid boundary segments *BFEA* and *DC* is zero because of the no-normal flow condition. $Q$ is the northward transport between $B$ and $C$ or between $A$ and $D$. It is also the net cyclonic transport through the marginal sea. $f_N$ and $f_S$ are planetary vorticity along *BC* and *AD*. *Godfrey* [1989] cleverly chose this integration path to avoid the viscous western boundary layer along the island's east coast (i.e., *AB* in Figure 1b). The friction, i.e., the third term on the right-hand side of equation (3), is therefore assumed to be negligible. He assumed the depth is constant and so the integral of the pressure torque around a closed path becomes zero. Equation (3) can be simplified to:

$$Q_{island-rule}=\frac{1}{\rho_0(f_N-f_S)}\oint_l\overrightarrow{\tau_w}\cdot d\vec{l}=\frac{1}{\rho_0\beta(y_N-y_S)}\oint_l\overrightarrow{\tau_w}\cdot d\vec{l} \tag{4}$$

[10] This is the original form of Godfrey's IR.

## 3. Topographic and Frictional Effects on the Island Rule

[11] In this section, we will discuss some topographic effects on the IR. If the model has a constant depth $h_0$, the two basins shown in Figure 1b are connected by geostrophic contours $f/h_0$ along which geostrophic currents flow freely. This geostrophic flow will be interrupted by a ridge between two basins. Ageostrophic processes or external forcing are needed for cross-ridge exchanges between two basins. This brings up an interesting question. Does friction, a major ageostrophic factor, actually promote interbasin flows? If so, the friction reverses its role from that in the original IR in which it always acts to reduce the throughflow transport [*Wajsowicz*, 1993; *Pedlosky et al*., 1997; *Pratt and Pedlosky*, 1998; *Seung*, 2003].

[12] A wind-driven barotropic model [*Yang*, 2007] is used here to examine these issues.

$$\begin{aligned}&\frac{\partial u}{\partial t}+\vec{u}\cdot\nabla u-fv=-g\frac{\partial\eta}{\partial x}+\frac{(\tau_w^x-\tau_f^x)}{\rho h}+\frac{A_H}{h}\nabla\cdot(h\nabla u)\\&\frac{\partial v}{\partial t}+\vec{u}\cdot\nabla v-fu=-g\frac{\partial\eta}{\partial y}+\frac{(\tau_w^y-\tau_f^y)}{\rho h}+\frac{A_H}{h}\nabla\cdot(h\nabla v)\\&\frac{\partial\eta}{\partial t}+\nabla\cdot(\vec{u}h)=0\end{aligned} \tag{5}$$

where $\eta$ is the SSH, $h$ is the total layer thickness, $\rho$ is the density, and $\vec{\tau}_w$ is the surface wind stress. A quadratic drag is used for the bottom stress, i.e.:

$$\overrightarrow{\tau_f}=\rho\lambda\sqrt{(u^2+v^2)}\vec{u} \tag{6}$$

where $\lambda=10^{-3}$ and $A_H=500\ \mathrm{m^2\ s^{-1}}$ are used for bottom and lateral frictions in the control run ($A_H$ and $\lambda$ will be

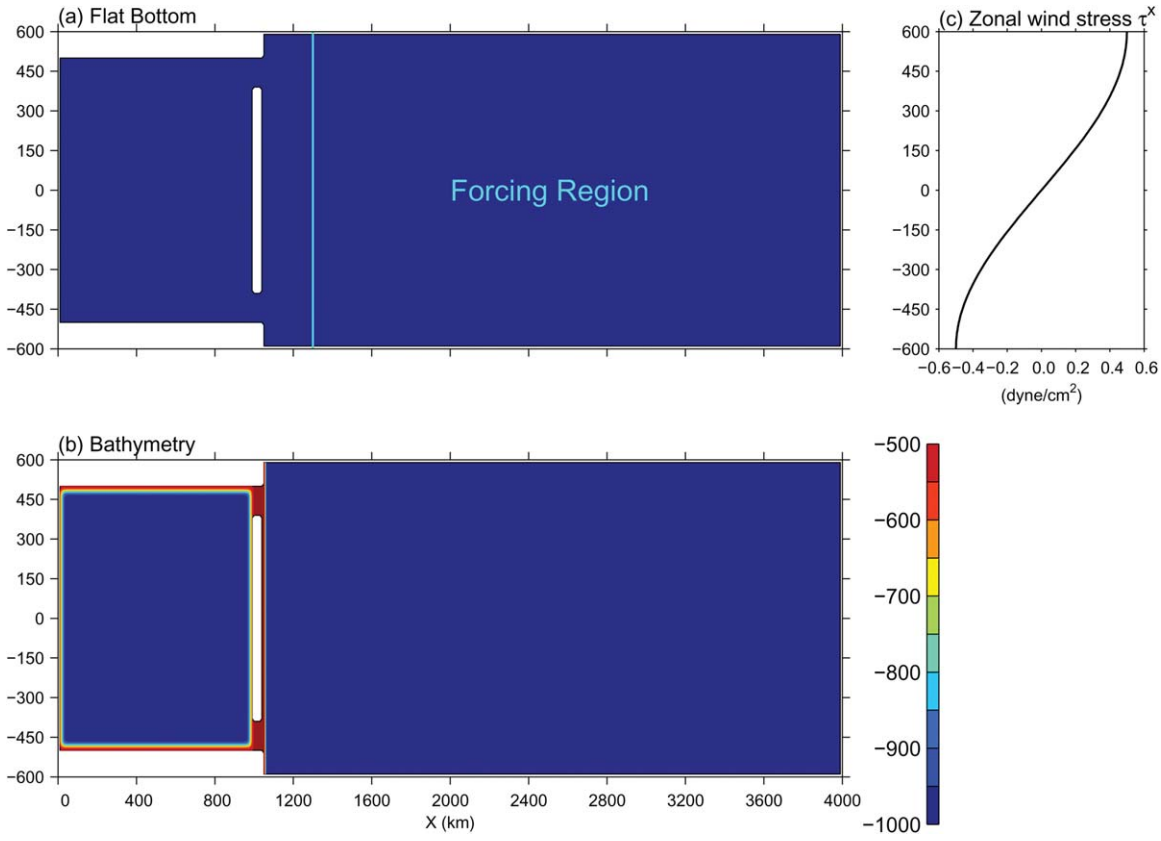


**Figure 2.** The bathymetry of the idealized model used in the first pair of experiments, (a) one with a flat bottom and (b) another with a ridge between two basins. The sill depth is 500 m in both straits, the width of both gaps is 120 km, and the deep basins are 1000 m in depth. It is found that the slope along the western boundary of the open ocean (right side basin) is an important parameter in the *ocean-sea* transport. In this first experiment, the slope is set to be $\alpha = 0.05$ ($h_0$ changes linearly from 500–1000 m over 10 km distance). A steeper slope will result in a greater transport over the sill between two basins and this will be discussed more in the paper. (c) The right plot is the zonal wind stress profile. The wind stress is applied only from $x = 1300$ to $x = 4000$ km and so the marginal sea and the vicinity of the island are not forced locally by wind stress.

varied in sensitivity experiments). The form of lateral friction was chosen to ensure that internal dissipation does not create or destroy momentum [*Schär and Smith*, 1993; *Helfrich et al.*, 1999]. The width of Munk layer, $(A_H/\beta)^{1/3}$, is about 30 km. The model is discretized by using the C-grid with a resolution of 5 km in space and 10 s in time. The no-slip and no-normal flow conditions are applied along all solid boundaries. The model uses the $\beta$-plane centered on 35°N. Most experiments are conducted in pairs, one with a flat bottom and the other with a ridge between the marginal sea and the open ocean (Figures 2a and 2b). The IR will be used to compare with numerical results. The deep basin depth in this highly idealized model is set to be 1000 m, which is much shallower than the depth in the deep ocean.

[13] In most experiments, the model is driven by the same forcing—a zonal wind stress which is shown in Figure 2c. The meridional wind stress is set to be zero everywhere. The forcing is applied only between $x = 1300$ km and 4000 km (Figure 2a), so the marginal sea and straits are not forced locally by wind stress. With this model configuration and wind stress, the IR equation (4) yields a transport of 15.4 Sv (1 Sv $= 10^6$ m$^3$ s$^{-1}$). In the first numerical experiment, we use flat bottom (Figure 2a). We have conducted experiments by using both the linear and the nonlinear versions of the model. In the linear model, all nonlinear terms, including the bottom friction, are set to be zero. The linear model produces a throughflow transport of 14.3 Sv, which is about 93% of what the IR yields (15.4 Sv). The good agreement is expected since the IR can be derived from the same numerical equation (except that the numerical model includes friction). In the fully nonlinear model with a bottom and a lateral friction, the transport is reduced to 13.5 Sv (Figure 3a shows the sea surface height, SSH)—about 88% of the IR result (15.4 Sv). Our analyses indicate that the reduction is due to both the bottom friction and the nonlinear advection term.

[14] What will happen to the throughflow if a ridge is placed between two basins in the model? We repeated the experiments by using the bathymetry shown in Figure 2b. A meridionally elongated ridge extends from the northern to the southern boundary and across two straits. The sill depth is set to be 500 m in both straits. The continental slope to the east of the island changes linearly from 500 to 1000 m over 10 km distance (the slope $\alpha = 0.05$) (Figure 2b). (It should

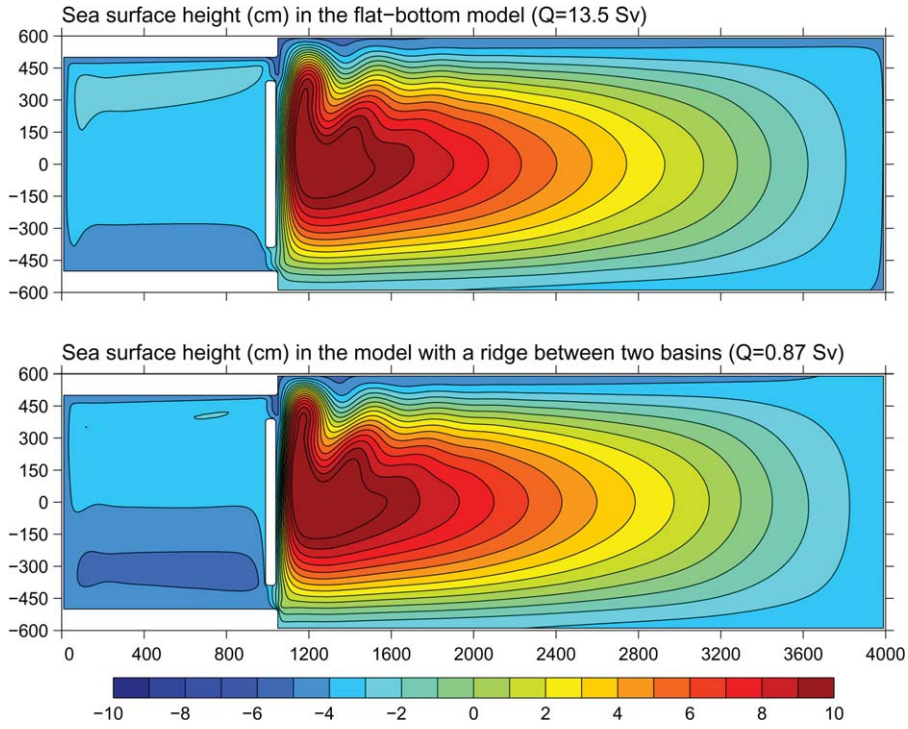


**Figure 3.** (a) The sea surface height (SSH) simulated in the first experiment using a fully nonlinear model and a flat bottom on the $\beta$-plane at 35N. The interbasin transport is 13.5 Sv (enters the marginal sea through the southern strait) which is about 88% of 15.4 Sv inferred from the island rule (4). A linear version of the model results in 14.3 Sv (93% of the island rule transport); (b) model result from using a bathymetry shown in Figure 2b. The transport is 0.87 Sv, much smaller than the flat bottom result or the island rule transport. The forcing is identical in both cases.

be noted that the slope was represented by two grids only in this model with a resolution of 5 km. We have repeated the same experiment by increasing the zonal resolution to 2.5 km. The result is virtually identical to that shown in Figure 3b.) Figure 3b shows the SSH from the nonlinear model run when forced by the same wind stress shown in Figure 2c. It is obvious that the interbasin exchange is much reduced. In fact, the throughflow transport is only 0.87 Sv. This is far less than that in the flat-bottom run (13.5 Sv) or that from the IR estimation (15.4 Sv). This indicates that even a modest ridge could significantly reduce the throughflow transport in a barotropic model.

### 3.1. Bottom Pressure Torque and Potential Vorticity Barrier

[15] The bathymetry affects two terms in the vorticity integral equation (3), the bottom pressure torque (the first term on the right-hand side of equation (1)) and the friction. The large discrepancy between the previous two experiments shown in Figure 3 must be due to either or both of them. The bottom pressure torque and its physical interpretation have been discussed in numerous literatures [e.g., *Mertz and Wright*, 1992; *Vallis*, 2006]. It exists in either a homogenous or a stratified fluid and is due to the torque of the pressure exerted on a varying bathymetry. This term in equation (3) is zero if the layer thickness is constant along $l$. In a barotropic model, this occurs if the integration is along a closed isobath or the model has a flat bottom like the first experiment shown in Figure 3a. In the second experiment, the integration path $l$ goes over the ridge and, therefore, the bottom pressure torque is no longer zero. In fact, the dominant balance in equation (3) is between the integrals of the pressure torque and the wind stress in the second experiment shown in Figure 3b according to our diagnoses.

[16] The role of the bottom pressure torque can be illustrated clearly in terms of the potential vorticity (PV) [*Vallis*, 2006]. It acts to steer flows along the geostrophic contours ($f/H$) and thus can be considered as a PV barrier that deters flows over the ridge between two basins. It is worth noting that a PV conserving water parcel can flow across geostrophic contours if the relative vorticity is large enough compensate the change of $f/H$ [e.g., *Whitehead et al*., 1974]. One can estimate the magnitude of relative vorticity if the water parcel conserves its PV that is set in a upstream deep basin, i.e.,

$$\frac{f+\zeta_{strait}}{H_{strait}} = \frac{f+\zeta_{ocean}}{H_{ocean}} \approx \frac{f}{H_{ocean}} \tag{7}$$

where $\zeta_{starit} \approx -\frac{\partial u}{\partial y}$ is the relative vorticity in a zonal strait (Figure 2) and the relative vorticity in the ocean, $\zeta_{ocean}$, is assumed to be small. The velocity shear in the strait is then estimated through the PV conservation equation, i.e.,

$$\frac{\partial u}{\partial y} = f\left(1 - \frac{H_{strait}}{H_{ocean}}\right) \tag{8}$$

[17] The Tsushima Strait has a maximum depth of about 150 m and 200 km in width. If we use $H_{strait} = 100$ m and

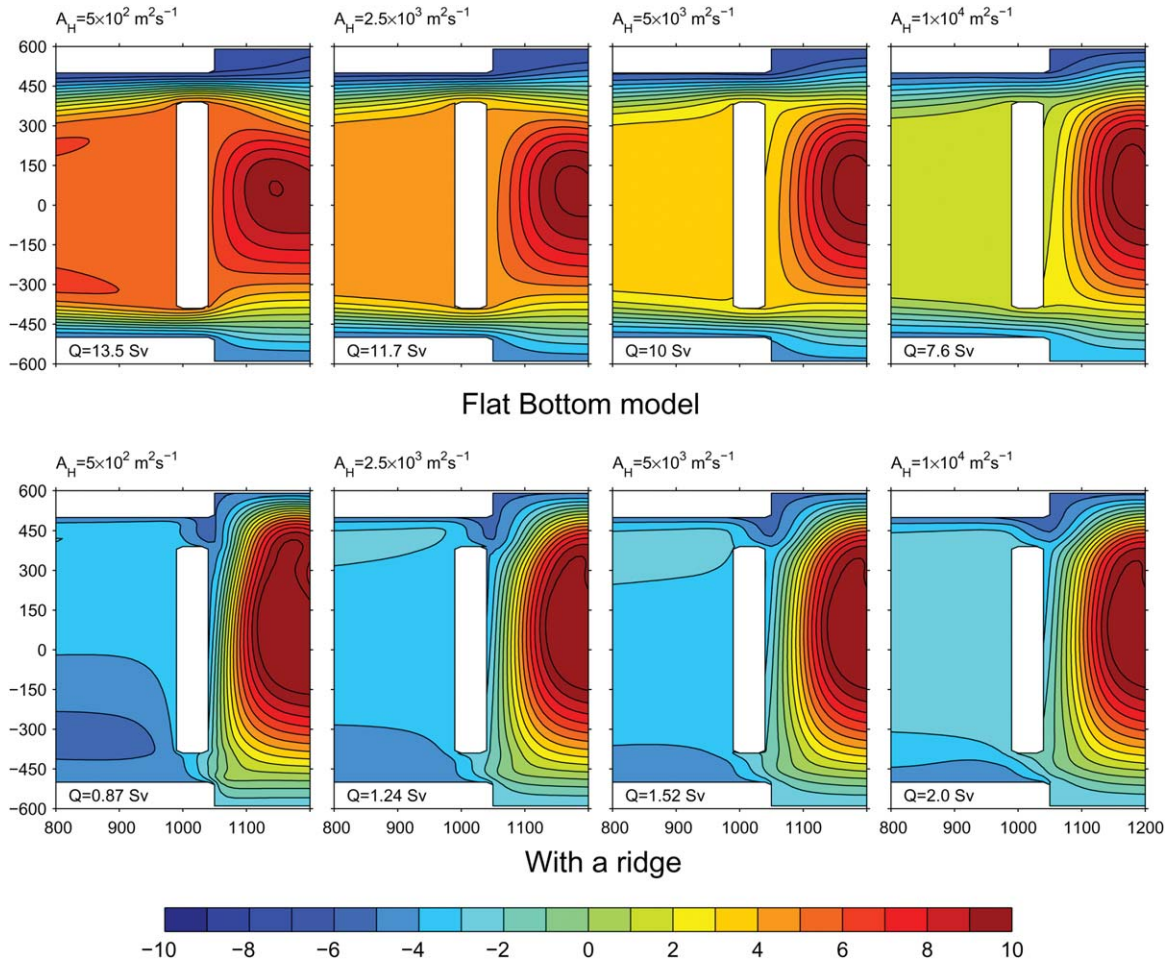


**Figure 4.** In the flat-bottom island rule, the interbasin transport decreases when the friction increases. This is supported in our model (see text). But change the viscosity (or the drag coefficient) over the whole basin affects the strength of the entire gyre. So we ran a series of experiments in which the viscosity is changed only between $x = 950$ km and 1100 km. (top) In the flat-bottom model, the transport between two basins decreases when the viscosity increases. (bottom) The model with a ridge, however, is opposite. The transport increases as the viscosity increases. The flow between two basins needs to overcome a PV barrier associated with the ridge. Friction is a main mechanism that promotes the transport across the PV isolines.

$H_{ocean} = 1000$ m, the velocity shear in the strait needs to be about $\frac{\partial u}{\partial y} \approx 7.5 \times 10^{-5} s^{-1}$ at 35°N in order to conserve PV. Repeated ADCP observations across the Tsushima Strait showed that the magnitude of relative vorticity is more than one order of magnitude smaller than what is needed for PV conservation [*Takikawa et al*., 2005]. So the PV is not likely to be conserved when going through a broad and shallow Tsushima Strait. This is different from some other overflows, such as the Nordic Seas overflows, where the PV is thought to be conserved when a water parcel overflows a sill [*Whitehead et al*., 1974].

### 3.2. The Role of Friction

[18] As discussed above, ageostrophic processes could help overcome the PV barrier and so could potentially promote a throughflow over the ridge and between two basins. Friction is a major ageostrophic process and its role is examined here. We have conducted several experiments using models with either a flat bottom or a ridge. When either $A_H$ or $\lambda$ increases, the throughflow transport decreases in the flat-bottom model (Figure 2a). In an experiment, for instance, we increased $A_H$ from 500 to 5000 m$^2$ s$^{-1}$ over the whole model domain while keeping all other parameters including $\lambda$ unchanged. The transport decreases from 13.5 to 8.4 Sv in the flat-bottom model. The results are consistent with the conclusions made by *Pedlosky et al*. [1997] and *Pratt and Pedlosky* [1998] that the friction tends to reduce the throughflow transport between two basins. The role of the friction, however, reverses when using the model with a ridge (Figure 2b). When $A_H$ is increased from 500 to 5000 m$^2$ s$^{-1}$, the throughflow transport increases from 0.87 to 1.3 Sv. So the friction plays an opposite role in models with and without a ridge.

[19] We note that changing the friction parameters ($A_H$ or $\lambda$) over the whole model domain affects the strength of the gyre in the open ocean. To focus the role of friction in overcoming the topographic barrier in the vicinity of the ridge, we have done another set of experiments in which

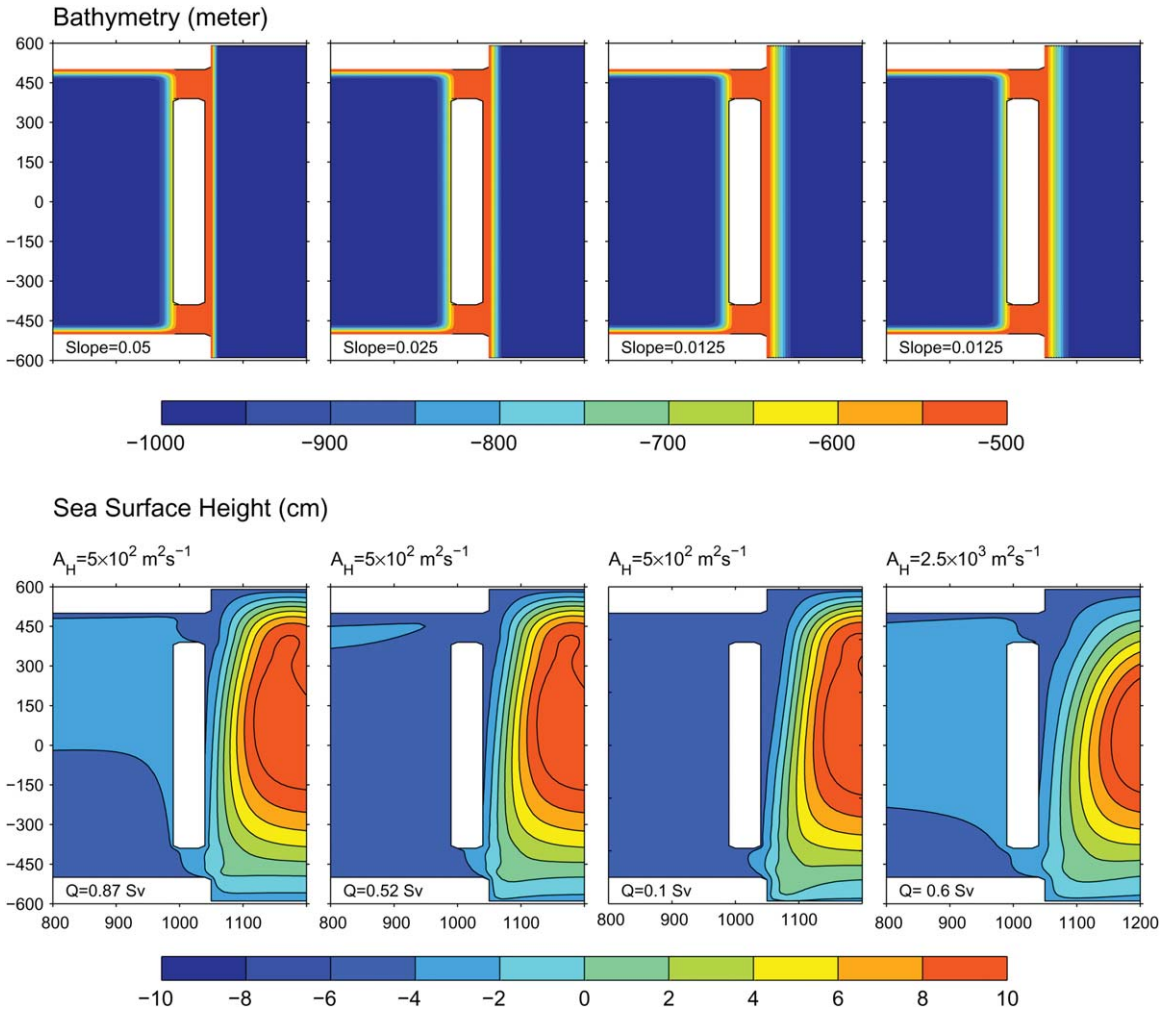


**Figure 5.** The slope on the eastern (oceanic) side of the ridge affects the width and intensity of the boundary current along the slope. So it affects the magnitude of the friction. A steeper slope narrows and intensifies the slope current. This results in a stronger shear and lateral friction, as well as bottom friction. So the transport is larger if the slope is steeper. (top) Three different slopes used in the model. (bottom) The corresponding transport.

either the lateral viscosity $A_H$ or the bottom drag coefficient $\lambda$ is amplified only in a narrow region between $x = 950$ and 1100 km. Outside this strip, the parameters are kept at the same values as those used in the control run (Figure 3), i.e., $\lambda = 10^{-3}$and $A_H$=500 m$^2$ s$^{-1}$. In this configuration, the strength of the open-ocean forcing, measured by the gyre strength, remains virtually the same as that in the control runs (Figure 3), and the frictional effect on the cross-isobathic transport is isolated.

[20] Figure 4 shows the model results from both flat-bottom (top row) and ridge-bottom (bottom row) model runs with four different viscosity used between $x = 950$ km and 1100 km. The interbasin transport in the flat-bottom model decreases from 13.5 Sv in the control run ($A_H = 5 \times 10^2$ m$^2$ s$^{-1}$) to 11.7 Sv ($A_H = 2.5 \times 10^3$ m$^2$ s$^{-1}$), 10 Sv ($A_H = 5 \times 10^3$ m$^2$ s$^{-1}$), and 7.6 Sv ($A_H = 1 \times 10^4$ m$^2$ s$^{-1}$). With a ridge, however, the transport is 0.87, 1.24, 1.52, and 2.0 Sv for $A_H = 5 \times 10^2$ m$^2$ s$^{-1}$, $2.5 \times 10^3$ m$^2$ s$^{-1}$, $5 \times 10^3$ m$^2$ s$^{-1}$, and $1 \times 10^4$ m$^2$ s$^{-1}$, respectively. The impacts are qualitatively the same when the bottom drag coefficient $\lambda$ is increased.

[21] The experiments show that the role of friction reverses when a ridge is placed between two basins. It dampens the throughflow transport in the flat-bottom case, consistent with previous studies [*Pedlosky et al.*, 1997; *Pratt and Pedlosky*, 1998] whereas it alleviates the topographic PV barrier and promotes transport over the ridge and between two basins even though it weakens the overall circulation in the eastern basin. It is interesting to note that this result is very different from that of *Minato and Kimura* [1980] and *Seung* [2003] who suggested that an enhanced friction in the shallow Tsushima Strait alone would be responsible for the small TSWC transport. The PV dynamics was not considered in their models.

[22] We should point out here that neither lateral viscosity nor the bottom drag coefficient is well quantified from observations. The eddy PV flux, explained by *Kida et al.* [2008, 2009] and *Spall* [2010], plays a leading role in permitting flow to cross the isobaths. We caution here that the uncertainty of using the eddy viscosity and drag coefficient values in this model is large. The results are valid only qualitatively.

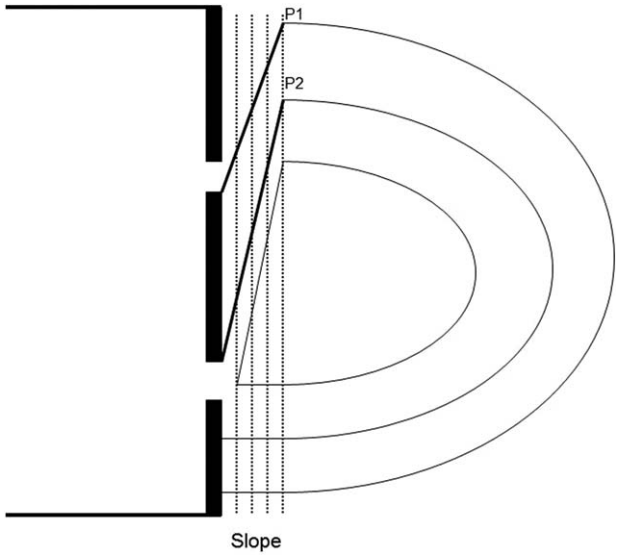


**Figure 6.** The schematic of how a continental slope (dashed lines for isobaths) affects the island rule. The eastward flow from the interior deflects southward and tends to follow the *f/h* contours. Friction and nonlinearity deviate the flow from *f/h* contours. The two thick lines are the streamlines that connect the two extremities of the island to the forcing latitudes $P_1$ and $P_2$ in the interior ocean. The transport between two basins is forced by wind stress along the latitudes of $P_1$ and $P_2$ in the open ocean instead of the latitudes of the island's extremities in the original island rule. The positions of $P_1$ and $P_2$ are determined by *f/h* values in two straits and affected by friction in the slope region.

## 4. Continental Slope and a Remote Forcing Mechanism

[23] Several additional experiments were conducted to examine the model sensitivity to the slope of the ridge. It was found that the throughflow transport in the model with a ridge is sensitive to the slope on the eastern side (facing the open ocean basin) of the ridge (i.e., off the coast $A'ABB'$ in Figure 1). Figure 5 shows three examples of using different slopes in this region while everything else is kept unchanged. The transport changes from 0.87 Sv (the control run) to 0.52 and 0.1 Sv, respectively, when the slope decreases from $\alpha = 0.05$ to $\alpha = 0.025$ and $\alpha = 0.0125$ (Figure 5). The exchange is basically shut off when $\alpha$ is smaller than 0.0125.

[24] The slope affects the width and thus the shear of the current along the continental slope and so the PV dissipation (the torque of the friction). To examine this, let us revisit the linear and steady balance of the vorticity in the slope region,

$$\vec{U}\cdot\nabla\left(\frac{f}{h}\right) = -curl_z\frac{\overrightarrow{\tau_f}}{\rho h} + curl_z\left[\frac{A_H}{h}\nabla\cdot(h\nabla\vec{u})\right] \qquad (9)$$

where $\vec{U} = h\vec{u}$is the vertically integrated velocity. The local wind stress is zero in the model slope region. Equation (9) states that the transport across PV isolines is driven by the torque of friction.

[25] When the flow from the interior ocean approaches the slope on the eastern side of the ridge, the water mass tends to flow along the geostrophic contours. The magnitude and the shear of the current are affected by the width of the slope, which is defined as

$$L_{slope} = \frac{\Delta H}{\alpha} \qquad (10)$$

where $\alpha$ is the slope and $\Delta H$ is the depth change across the slope. In our model configuration, the isobathic lines are meridional on the ocean side of the ridge. The meridional scale is much greater than the width of the slope and the flow is mainly in the meridional direction along *f/H* isolines. The vorticity equation (9) can then be simplified to:

$$\vec{U}\cdot\nabla\left(\frac{f}{h}\right) \approx -\lambda\frac{\partial}{\partial x}\frac{|v|v}{h} + A_H\frac{\partial}{\partial x}\left\{\frac{1}{h}\left[\frac{\partial}{\partial x}\left(h\frac{\partial v}{\partial x}\right)\right]\right\} \qquad (11)$$

[26] A scaling analysis of equation (11) indicates that the first and second terms on the right-hand side of equation (11) are proportional to $L_{slope}^{-1}$ and $L_{slope}^{-3}$ (or $\alpha$ and $\alpha^3$), respectively. So the torque of the friction available for the transport across *f/h* contours decreases with a greater width $L_{slope}$ or a smaller slope $\alpha$. This may help to explain why the throughflow transport decreases when the slope becomes less steep in our barotropic model. When $L_{slope} >$ 250 km, the slope extends into the region of wind-stress forcing (i.e., $x \geq$ 1300km). Transport across geostrophic contours is affected by both friction and wind stress. The sensitivity of the transport to $L_{slope}$ or $\alpha$ is no longer determined by friction only.

[27] As mentioned in the previous section, both lateral and bottom frictions are not well quantified in the real ocean and poorly represented in numerical models like ours. They are related to small and mesoscale scale features, such as eddies. *Kida et al*. [2008, 2009] used a two-layer isopycnal model and demonstrated that a dense-water flow across continental slope is forced by flux of eddies. Similarly, *Spall* [2010] used an eddy-resolving 3-D model and found that transports across isobaths along a continental slope are carried out mainly by eddies. In Spall's model, the intensity of eddies or the eddy transport increases when the $L_{slope}$ narrows. Our result is consistent with his finding. But the agreement is only qualitatively at best since our model does not include baroclinic processes that are essential for eddies in Spall's model.

[28] Figure 5 shows that the transport is nearly zero when the western boundary current does not intercept the east coast of the island (the third case where $A_H = 500$ m$^2$ s$^{-1}$ and $\alpha = 0.0125$). If the $L_{slope}$ is broad and friction is small, the flow within the slope region would deviate little from *f/h* isolines and the slope current flows southward before reaching the southern strait. In this case, there is no current along the east coast of the island and thus no throughflow between two basins. When the friction is enhanced, such as in the fourth case shown in Figure 5, the flow in the slope region deviates more from the *f/h* isolines and intercepts the island's east coast. This results in a nontrivial transport between basins. The result suggests a latitudinal shift in the open ocean area as illustrated in Figure 6. The flow along the east coast of the island is affected by gyre circulation within the latitude of $P_1$ and $P_2$ in the open

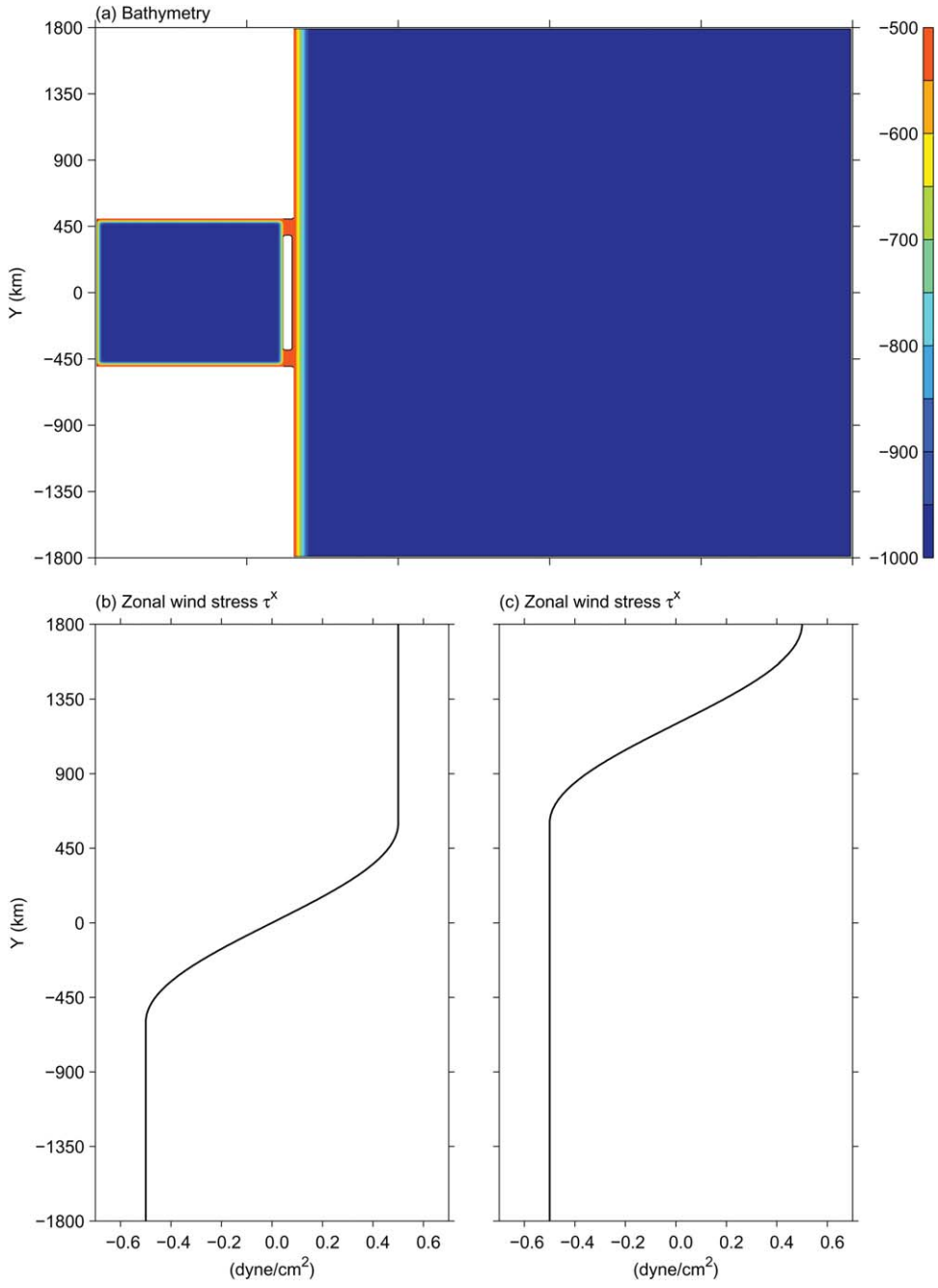


**Figure 7.** A larger model domain is used to illustrate a remote forcing mechanism. Two zonal wind stress profiles are used.

ocean (Figure 6). Wind-stress forcing outside this latitudinal range has no direct impact on exchanges through either strait.

[29] To illustrate this latitudinal shift in the open-ocean forcing, we ran another set of experiments by using a larger oceanic domain, one with a ridge as shown in Figure 7a and another with a flat bottom ($h = 1000$ m). The reason for using such a bigger domain is to permit a larger latitudinal range, i.e., $P_1$ and $P_2$ in Figure 6, so that the remote forcing can be better illustrated. In this set of experiments, we use a small slope $\alpha = 0.0125$ on the eastern side of the ridge and a larger viscosity $A_H = 2000$ m$^2$ s$^{-1}$ (compared with $A_H =$ 500 m$^2$ s$^{-1}$ in the control run Figure 3a). Using a larger viscosity allows the remote forcing latitudes, i.e., $P_1$ and $P_2$ in Figure 6, to be within the model domain (when $A_H$ decreases the cross-PV velocity weakens, so $P_1$ and $P_2$ moves further away from latitudes $y_S$ and $y_N$). Two sets of zonal wind stress are used. The first one has a nonzero curl, $-\partial\tau^x/\partial y$, within the range of $-600$ km $\leq y \leq 600$ km (Figure 7b), whereas the second one has a nonzero curl in the northern 1/3 of the domain (i.e., $y \geq 600$ km, Figure 7c).

[30] The SSH fields from the flat-bottom model are shown in the top plots in Figure 8. In the first case with wind stress shown in Figure 7b, there is an anticyclonic

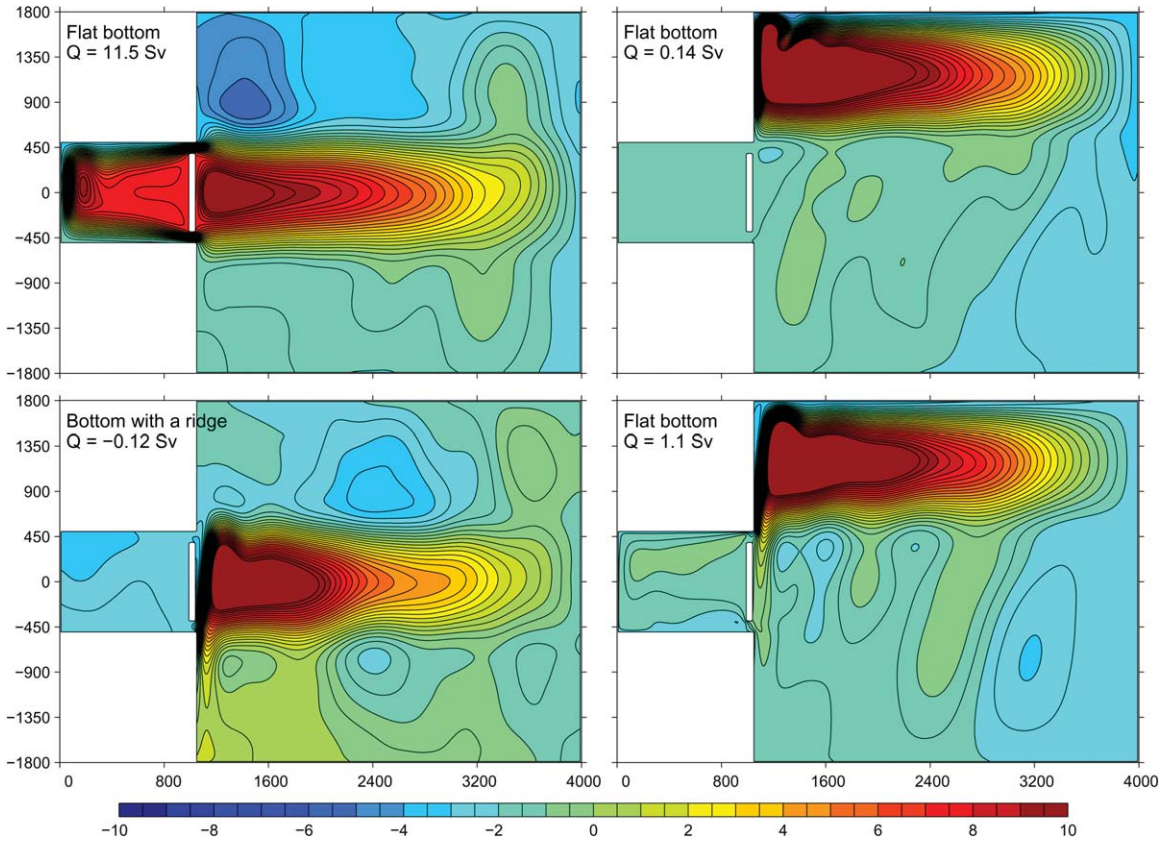


**Figure 8.** (top) The model results of using the flat-bottom model and (bottom) a ridge-bottom model. There is a large anticyclonic gyre to the east of the island when forced by the first wind stress profile. The interbasin transport is 11.5 Sv in the flat-bottom model and 0.12 in the model with a ridge. The island rule transport is 15.4 Sv. In the second wind-stress forcing, there is a cyclonic gyre in the open ocean north of the marginal sea latitude. The transport in the flat-bottom model is 0.14 Sv—close to the zero transport inferred from the island rule (4). The transport in the model with ridge, however, is 1.1 Sv. These experiments demonstrate that the forcing region in the open ocean is shifted by the ridge.

gyre just to the east of the marginal sea (Figure 8, top left). The exchange transport between two basins is 11.5 Sv, about 75% of the transport calculated from the IR (15.4 Sv). It is also smaller than the model transport in a previous experiment that uses a smaller basin with the same wind-stress forcing (13.5 Sv, Figure 3a). Our analyses indicate that the use of a larger viscosity ($A_H$ =2000 m$^2$ s$^{-1}$ versus $A_H$ = 500 m$^2$ s$^{-1}$ in the standard run shown in Figure 3) in the whole model domain is the main cause for the weaker transport. In the second wind-stress profile, the region of positive curl is moved northward to the northern 1/3 of the basin as shown in Figure 7c. The open ocean is dominated by a large anticyclonic gyre in the northern 1/3 of the model domain (Figure 8, top right). The transport through each strait is nearly zero (0.14 Sv). The model result is consistent with the IR that gives a zero transport since the wind stress is zero between $y_S$ and $y_N$.

[31] With a ridge between the two basins (Figure 7a), the exchange between two basins in the model is very different. The throughflow transport is very small (0.12 Sv) in the first case with an anticyclonic gyre to the east of the marginal sea (Figure 8, bottom left). This is consistent with a previous experiment that used a gentle slope in a smaller basin, i.e., the third experiment shown in Figure 5. Therefore, the ridge shields the marginal sea form the wind-stress forcing in the open ocean. The situation changes when the open ocean gyre is forced by the second wind stress profile (Figure 8, bottom right). This forcing induces a transport of 1.1 Sv exchange between two basins. The experiments here show a key difference between the IR and the model with a ridge between two basins. In the original IR, the transport depends on only the wind stress along the two latitudinal extremities of the island, i.e., $y_N$ and $y_S$ in Figure 1b. But in the case with a ridge the latitudes of the open-ocean forcing, i.e., $P_1$ and $P_2$ in Figure 6, is shifted meridionally. The exact positions depend on a number of topographic and physical factors, including the slope on the island's east coast and frictions. If the flow is inviscid, position of $P_1$ and $P_2$ are determined by $f/h$ values set at the northern and southern tips of the island.

[32] Does the remote forcing mechanism apply to the Japan/East Sea? The JES is located between the latitudinal range of the North Pacific Subtropical and Subpolar Gyres. Will the result here imply that the TSWC is forced by the subpolar gyre through the Oyashio Current instead of by the subtropical gyres through the Kuroshio Current? The bathymetry to the east of Japan is complicated as shown in Figure 9a. The $L_{slope}$ is narrow as slope becomes steep to

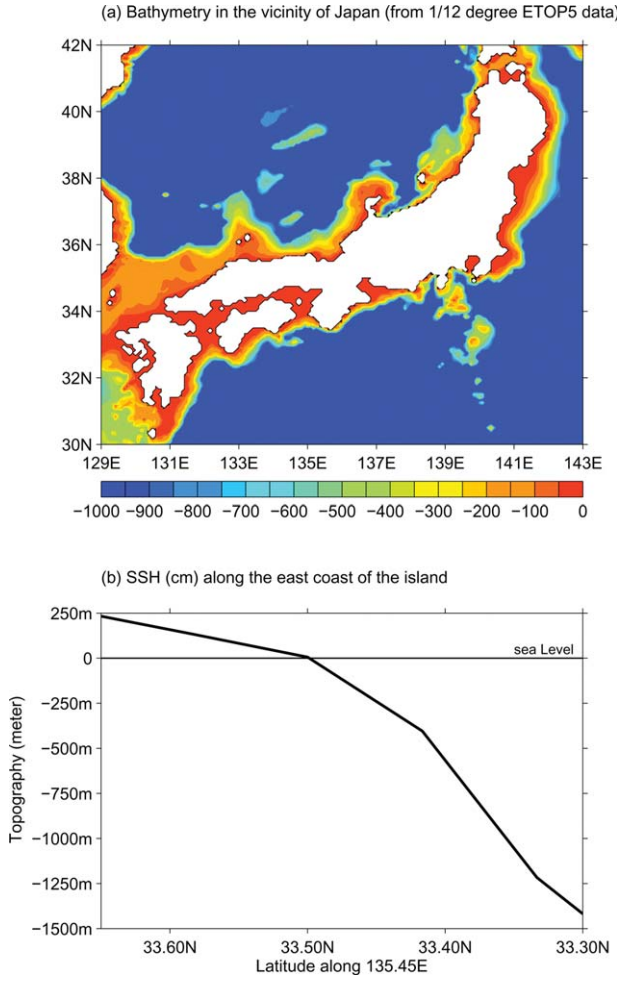


**Figure 9.** The bathymetry around Kyushu and Honshu between the Tsushima and Tsugaru Straits. Along the east coast, the slope is steep to the south of 35N. It becomes gentler to the north of that latitude. (bottom) The profile of bathymetry along 135.45E. The water depth changes from 0 to 1400 m in about 20 km along the 135.45E (using the 1/12 degree ETOPO5 data)—a slope of 0.07, which is greater than that shown in Figure 3.

the south of 35N. Figure 9b shows that the water depth changes from 0 to 1400 m over a distance of about 20 km along the 135.45E (using the 1/12 degree ETOPO5 data)—a slope of 0.07, which is greater than what has been used in the control run (Figure 3b) in this study. With this steep slope, the Kuroshio Current could probably force the TSWC effectively. So this remote forcing mechanism is probably ineffective for the TSWC through JES. Numerical experiments using a 3-D model indeed show that the TSWC is forced directly by the Kuroshio Current [*Ma et al.*, 2010].

## 5. Latitudinal Dependence of the PV Barrier Effect

[33] Previous applications of the IR in the SCS [*Wang et al.*, 2006a, 2006b] yielded transport estimates that are broadly within the observed one despite of multiple passages through the Philippines. The throughflow exits the SCS mainly through the Karimata Strait (<50 m) and the remaining through Mindoro Strait (<200 m) [*Qu et al.*, 2005]. It's beyond the scope of this idealized study to test the IR applicability in a basin with such a complex geography. We are nevertheless interested in why the shallowness of Karimata and Mindoro Straits do not seem to affect the throughflow as severely as those in the JES. Does their proximity to the equator play a role? To examine this, let's reconsider the bottom pressure torque:

$$Q_{torque} = \frac{1}{\rho_0 \beta (y_N - y_s)} \oint_l \left[ -h \left( \nabla p_b \cdot \vec{l} \right) \right] ds = \frac{1}{\beta (y_N - y_s)} \oint_l \left[ hf \vec{u}_{geostrophic} \cdot \vec{n} \right) ] ds \quad (12)$$

where $\vec{u}_{geostrophic}$ is the geostrophic velocity above the bottom Ekman layer. When a geostrophic current moves toward the equator, e.g., from the Luzon Strait to Karimata Strait, the pressure gradient decreases because the Coriolis parameter $f$ becomes smaller. The bottom torque exerted by this geostrophic pressure gradient becomes negligible when the geostrophic current is close to the equator. This can also be understood in terms of distribution of $f/h$, which is zero at the equator regardless of water depth $h$. In this case, the ridge is no longer a PV barrier for interbasin flows.

[34] To test this latitudinal dependence, we ran another set of model experiments with identical forcing and bathymetry as in the first set of experiments shown in Figure 3, except that the $\beta$-*plane* is now moved to 6°N (instead of 35°N in Figure 3). The whole model domain is still in the northern hemisphere with $f > 0$. The straits, especially the southern one, are close to the equator. Figure 10 shows the SSH field for the flat-bottom and ridge-bottom cases, respectively. The throughflow transport in the flat-bottom model (11.6 Sv) is still higher than that in the ridge-bottom model (6.4 Sv). The impact of the ridge, however, is much smaller than that in the mid-latitude (Figure 3). The transport inferred by the IR equation (4) is 12.8 Sv on a $\beta$-plane centered at 6°N and is smaller than 15.4 Sv in the previous case at 35°N (the IR transport is proportional to $1/\beta$).

[35] The transport with a ridge is still considerably smaller than the IR transport (Figure 10). We note that the northern strait is located still considerably far away from the equator and $f$ is not small (it varies from $f = 2.4 \times 10^{-5}$ to $f = 2.7 \times 10^{-5} s^{-1}$ in northern strait). So the topographic PV barrier is still effective in the northern strait. In the SCS, the northern strait, i.e., the Luzon Strait, is deep and so the PV barrier is small even though $f$ is not small. To show that, we conducted another set of experiments in which the northern strait is deep (Figure 11a) like the Luzon Strait. Again, we run the model on $\beta$-planes at both 6°N and 35°N. On the 35°N $\beta$-plane, the transport between two basins is 1.6 Sv, larger than the case in which both straits are shallow (0.87 Sv in Figure 3b) but still substantially smaller than the IR transport (15.4 Sv). This indicates that the throughflow transport in a marginal sea outside the tropics can be effectively blocked by a shallow sill in one strait instead of in both. On the 6°N $\beta$-plane, however, the throughflow transport reaches as high as 11.2 Sv. It is virtually the same as the flat-bottom model case (11.6 Sv) shown in Figure 10 and is also much closer to the IR-estimated one (12.8 Sv). The PV barrier associated with

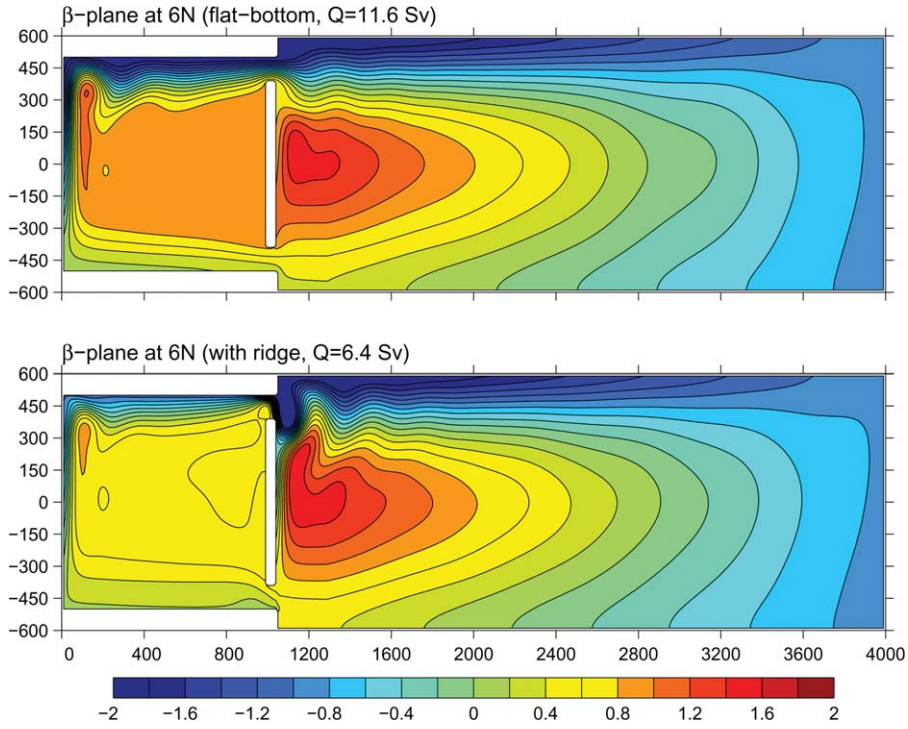


**Figure 10.** Same as Figure 3 except that the $\beta$-plane is moved closer to the equator from 25N to 6N. The difference between the flat-bottom and ridge-bottom models is much smaller than that from 35N $\beta$-plane. The transport from the island rule (4) is 12.8 Sv on this 6N $\beta$-plane. There remains a large gap between the model with a ridge and the island rule solution. This is because *f/h* variation is no longer small across the northern strait. So the PV barrier is effective there. If the shallow strait is close the equator, the result is much closer to the island rule (see Figure 11c).

the shallow bathymetry in the southern strait is ineffective due to the fact that the planetary vorticity is nearly zero there ($f = 3.8 \times 10^{-6} to\ f = 6.4 \times 10^{-6} s^{-1}$ in the southern strait). In summary, the topographic PV barrier weakens near the equator.

## 6. The Limitation of the Barotropic Island Rule and Some Potential Effects of Stratification

[36] In this study, we have examined some topographic effects on steady transports through semienclosed marginal seas. The vorticity equation (1) or a generalized IR equation (3) can be derived from either a 3-D model or a one-layer barotropic model. Both the bottom pressure torque, $curl_z(h\nabla p_b)$, and the bottom friction, $\tau_f$, are related to the bottom pressure gradient (or the geostrophic velocity above the bottom boundary layer). For a 3-D flow, the bottom pressure consists of both baroclinic and barotropic components. In an equilibrium state, the barotropic and baroclinic pressure gradients tend to cancel each other in the abyssal ocean below the level of no motion. Both the bottom pressure torque and the bottom friction would become zero, and the flow above the level of no motion is no longer influenced by topography and bottom friction. In a barotropic model, both the bottom friction and pressure torque exist even in an equilibrium state as long as the barotropic velocity is not zero. In the TSWC case, the topographic effect likely remains effective since the all connecting straits to the JES are very shallow (<200 m) and the sills are above the level of notion. Using a *f*-plane coastal model, *Brink* [1998] showed that the geostrophic flow in a stratified ocean may have large shear in vertical but the whole water column is still strongly steered by bottom topography. So this topographic effect may remain effective even for deep ridges if the cross-slope flows occur on scales that the planetary $\beta$ is small.

[37] For time-dependent throughflows, the topographic PV barrier effect could still be relevant in a 3-D flow even if the bathymetric variation is below the level of no mean motion (i.e., the long-term averaged velocity is zero). The depth-integrated transport of an oceanic gyre is established nearly instantaneously (on a time scale of days for an oceanic basin) in response to wind-stress forcing. It would take years even decades for baroclinic processes to shut down flows in abyssal oceans and establish a depth of no motion. Before that, an oceanic circulation would still interact with the bottom bathymetry and the PV barrier could still be effective. So it is possible, the topographic PV barrier below the level of no mean motion would continue to exert some influences on slowly varying throughflows on the time scales between the fast barotropic (days) and slow baroclinic (years to decades) adjustment time scales. These remain as speculative until they are examined in a 3-D model. The main purpose of this study is to develop some basic insights that can be useful for future investigations.

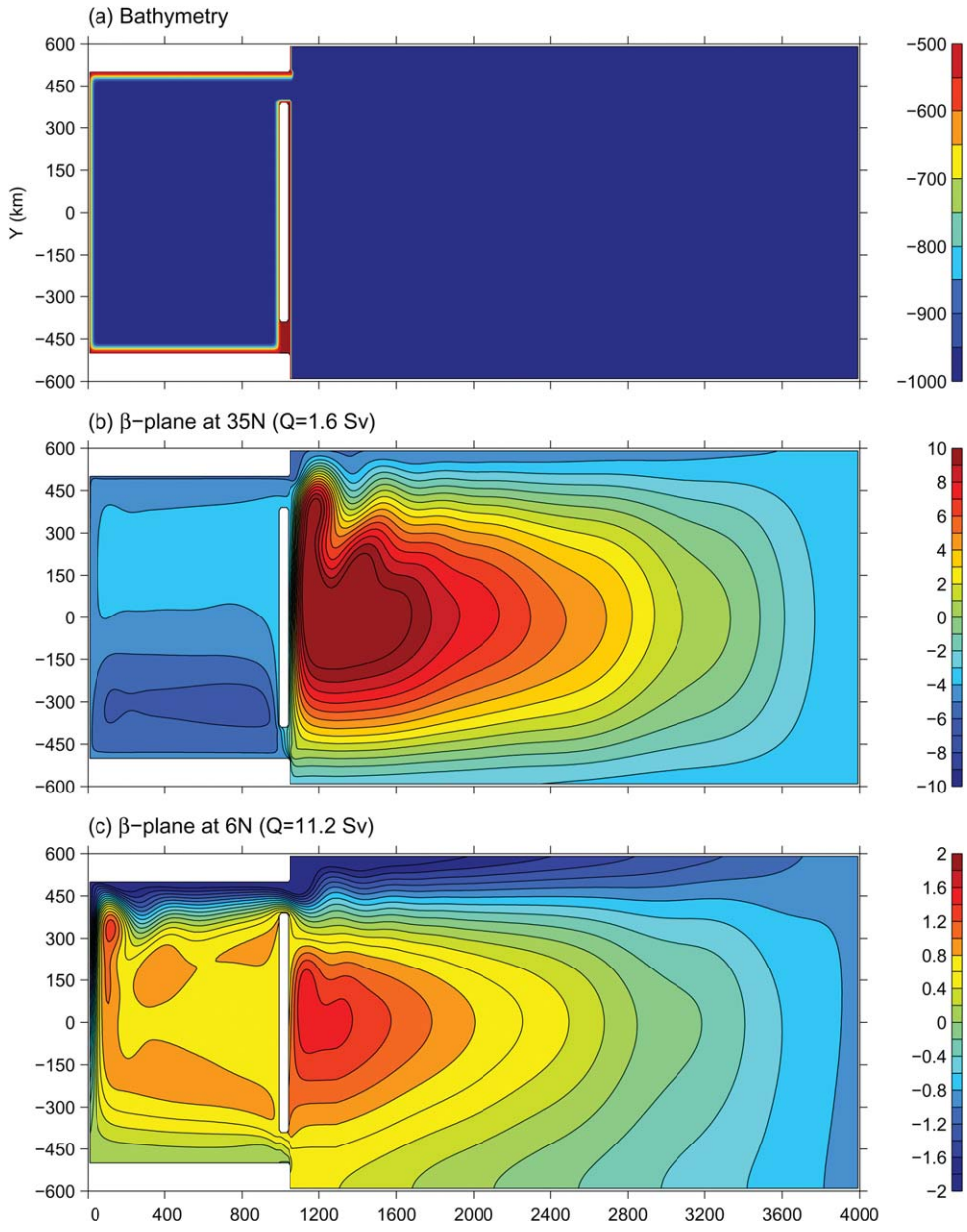


**Figure 11.** This experiment is used to show that the PV barrier in a single strait can be effective in blocking the interbasin transport. (a) The bathymetry with one deep and one shallow strait; (b) result from the 35N $\beta$-plane; and (c) result from the 6N $\beta$-plane. On the 35N $\beta$-plane, the southern strait represents an effective PV barrier and so the transport is much smaller than the island rule solution (1.6 Sv versus 15.4 Sv). On the 6N $\beta$-plane, the shallow strait (southern) is very close to the equator, and so the transport is close to the island rule solution (11.2 Sv versus 12.8 Sv).

## 7. Summary and Discussion

[38] In this study, we examine some topographic effects on transports between the open ocean and a semienclosed marginal sea. We used a one-layer barotropic model that is forced by a zonal wind stress over the open ocean. In a flat-bottom model, the modeled transport between two basins agrees reasonably well with that inferred from the IR. The throughflow transport weakens substantially once a ridge is placed between the open ocean and the marginal sea. The reduction is mainly due to the topographic PV barrier effect that can be represented by the bottom pressure torque (or the form drag) in a more generalized IR formulation. Friction helps overcome the PV barrier and promote the transport from one basin to the other. Using a larger viscosity or bottom drag coefficient in the model leads to a greater throughflow transport in the model with a ridge. This is the opposite of what friction does in a flat-bottom model in which the friction always tends to weaken the throughflow transport.

[39] The slope of the ridge sets the width of the slope current, affects the shear and velocity along the slope and thus affects the magnitude of the friction. It is an important factor that influences the transport between basins. When a zonal flow approaches the ridge from the ocean interior, it deflects to be along geostrophic contours. A steeper slope narrows the current's width scale and increases its shear. The friction is enhanced and the transport over the ridge is increased. We have examined a remote forcing mechanism that is associated with the presence of the ridge (or trench). In the original IR, the throughflow transport is forced by the wind stress solely within the latitudinal range between the northern and southern tip of the island. Forcing outside this latitudinal range does affect the IR transport. When there is a ridge, however, the forcing range is shifted and is determined by *f/h* in two connecting straits and the intensity of friction.

[40] The PV barrier effect depends on the latitudinal positions of the connecting straits. If a strait is located near the equator, the pressure gradient associated with an equatorward geostrophic current becomes smaller and so does the bottom pressure torque. Numerical experiments show that a shallow sill in a strait close to the equator does not affect the throughflow transport. We discuss the limitation of our barotropic model and some potential effects of stratification. The bottom pressure torque is zero if the bottom pressure gradient vanishes. Deep ridges or trenches below the depth of no motion do not likely affect steady exchanges between two basins.

[41] Previous studies have used the TSWC as an example to study wind-driven throughflow between an open ocean and a marginal sea [*Minato and Kimura*, 1980; *Nof*, 1993; *Seung*, 2003]. In an influential study, *Minato and Kimura* [1980] studied barotropic flows in a domain that consists of two flat-bottomed basins, a deep open ocean and a shallow marginal sea, that are connected by two sloping straits. Their result, however, is very different from ours. Wind stress is applied only in the open ocean basin as in ours. They derived an analytical solution by using the *Stommel* [1948] solution in the two flat-bottomed basins and modified it to satisfy flows with two connecting channels. They made a number of assumptions, which include that the flow is uniform across each channel and the pressure gradient is balanced by friction in the along-channel direction, in their derivation. The topography affects mainly the friction within two channels. The analytical solution is complex but the essential dynamics is actually rather straightforward. The negative curl of wind stress in the flat-bottomed ocean basin forces an inflow at the entrance of the southern strait. This flow is resisted by enhanced friction in the shallow straits and marginal sea. So the throughflow transport decreases as the friction increases. In essence, their solution is an island rule transport that is weakened by enhanced frictions in the shallower straits and marginal sea. We emphasize the different roles that topography and friction, i.e., the topography blocks geostrophic contours from connecting two basins and friction promotes ageostrophic flow over the sills.

[42] *Nof* [1993], on the other hand, considered an inviscid througflow in a reduced-gravity model without topographic effects. He found that the transport is dependent on the latitude of the connecting strait and the latitude of the Kuroshio Current's separation position. Interestingly, the transport increases toward lower latitude. This was used to *Nof* [2000] to explain why the transport into the Caribbean Sea is much larger than that into the JES. While this latitudinal dependence is similar to ours, the dynamics is very different. In our model, the larger transport in a lower latitude is due to a smaller topographic $\beta$ effect or smaller topographic PV barrier. This effect plays no role in a model without bathymetric variations like Nof's model. In a realistic TSWC model, both effects are likely coexisting and their relationship will be investigated in future studies.

[43] **Acknowledgments.** This study has been supported by the National Science Foundation grants OCE 1028739, OCE 0927017, ARC 1107412, and ARC 0902090 (J.Y.), the WHOI Coastal Institute, and by the Ministry of Education's 111 Project (B07036), National Basic Research Priorities Programmer (2013CB956202), Natural Science Foundation (41222037, 41221063), Natural Science Foundation of Shandong (JQ201111), and Public Welfare Scientific Research Project (201205018) of China (X.L. and D.W.). We thank Joe Pedlosky, Larry Pratt, and two reviewers for their comments.

## References

Brink, K. H. (1998), Deep-sea forcing and exchange processes, in *The Sea, The Global Coastal Ocean: Processes and Methods*, vol. *10*, edited by K. H. Brink and A. R. Robinson, Wiley, New York.

Godfrey, J. S. (1989), A Sverdrup model of the depth-integrated flow from the world ocean allowing for island circulations, *Geophys. Astrophys. Fluid Dyn.*, *45*, 89–112.

Helfrich, K. R., A. C. Kuo, and L. J. Pratt (1999), Nonlinear Rossby adjustment in a channel, *J. Fluid Mech.*, *390*, 187–222.

Kida, S., J. Price, and J. Yang (2008), The Upper-oceanic response to overflows: A mechanism for the Azores Current, *J. Phys. Oceanogr.*, *38*, 880–895.

Kida, S., J. Yang, and J. Price (2009), Marginal-sea overflow and upper-ocean interaction, *J. Phys. Oceanogr.*, *39*, 387–403.

Ma, C., D. Wu, X. Lin, J. Yang, and X. Ju (2010), An open ocean forcing in the East China and Yellow Sea, *J. Geophys. Res.*, *115*, C12056, doi:10.1029/2010JC006179.

Mertz, G., and D. G. Wright (1992), Interpretation of the JEBAR term, *J. Phys. Oceanogr.*, *22*, 301–305.

Minato, S., and R. Kimura (1980), Volume transport of the western boundary current penetrating into a marginal sea, *J. Oceanogr. Soc. Jpn.*, *36*, 185–195.

Nof, D. (1993), The penetration of Kuroshio water into the Sea of Japan, *J. Phys. Oceanogr.*, *23*(5), 797–807.

Nof, D. (2000), Why much of the Atlantic circulation enters the Caribbean Sea and very little of the Pacific circulation enters the Sea of Japan, *Prog. Oceanogr.*, *45*(1), 39–67.

Ohshima, K. I. (1994), The flow system in the Japan Sea caused by a sea level difference through shallow straits, *J. Geophys. Res.*, *99*, 9925–9940, doi:10.1029/94JC00170.

Pedlosky, J., L. Pratt, M. Spall, and K. Helfrich (1997), Circulation around islands and ridges, *J. Mar. Res.*, *55*, 1199–1251.

Pratt, L., and J. Pedlosky (1998), Barotropic circulation around islands with friction, *J. Phys. Oceanogr.*, *298*, 2148–2162.

Qu, T., Y. Du, G. Meyers, A. Ishida, and D. Wang (2005), Connecting the tropical Pacific with Indian Ocean through South China Sea, *Geophys. Res. Lett.*, *32*, L24609, doi:10.1029/2005GL024698.

Schär, C., and R. B. Smith (1993), Shallow-water flow past isolated topography. Part I: Vorticity production and wake formation, *J. Atmos. Sci.*, *50*, 1373–1400.

Seung, Y. H. (2003), Significance of shallow bottom friction in the dynamics of the Tsushima Current, *J. Oceanogr.*, *59*, 113–118.

Spall, M. A. (2010), Non-local topographic influences on deep convection: An idealized model for the Nordic Seas, *Ocean Modell.*, *32*, 72–85.

Stommel, H. (1948), The westward intensification of wind-driven ocean currents., *Trans., Am. Geophys. Union*, *2*(2), 202–206.

Takikawa, T., J.-H. Yoon, and K.-D. Cho (2005), The Tsushima Warm Current through Tshushima Straits estimated from ferryboat ADCP, *J. Phys. Oceanogr.*, *35*, 1154–1168.

Vallis, G. K. (2006), *Atmospheric and Oceanic Fluid Dynamics*, 745 pp., Cambridge Univ. Press.

Wajsowicz, R. (1993), The circulation of the depth-integrated flow around an island with application to the Indonesian throughflow, *J. Phys. Oceanogr.*, *23*, 1470–1484.

Wang, D., Q. Liu, R. X. Huang, Y. Du, and T. Qu (2006a), Interannual variability of the South China Sea throughflow inferred from wind data and an ocean data assimilation product, *Geophys. Res. Lett.*, *33*, L14605, doi:10.1029/2006GL026316.

Wang, Y., G. Fang, Z. Wei, F. Qiao, and H. Chen (2006b), Interannual variation of the South China Sea circulation and its relation to El Nino, as see from a variable grid global ocean model, *J. Geophys. Res.*, *111*, C11S14, doi:10.1029/2005JC003269.

Whitehead, J. A., A. Leetma, and R. A. Knox (1974), Rotating hydraulics of strait and sill flows, *Geophys. Fluid Dyn.*, *6*, 101–125.

Woodgate, R. A., and K. Aagaard (2005), Revising the Bering Strait freshwater flux into the Arctic Ocean, *Geophys. Res. Lett.*, *32*, L02602, doi:10.1029/2004GL021747.

Yang, J. (2007), An oceanic current against the wind: How does Taiwan Island steer warm water into the East China Sea?, *J. Phys. Oceanogr.*, *37*, 2563–2569.